Program Digest, 2019 IEEE International Ultrasonics Symposium (IUS)
Glasgow, Scotland, October 6-9, 2019

Development of ultrasensitive Doppler imaging method for the surgical management of open-brain tumors

C. Barthélémy[1], E. Koury[1], S. Beuve[1], I. Zemmoura[1], JL. Gennisson [2],
A. Bassarab[3], D. Kouamé[3], JP. Remeniéras[1]

[1]UMR 1253, iBrain, Université de Tours, Inserm, Tours, France.
[2]IRM Médicale et Multi-Modalités, CNRS UMR8081,Université Paris Sud,, CEA Service Hospitalier Frédéric Joliot, France.
[3]IRIT, Université de Toulouse, France.

***Abstract*—Gliomas are infiltrating tumors in the healthy brain parenchyma with no clear boundaries and can be located near or within "functional" brain zones driving as an example, motor skills, sensitivity, cognition or vision. Two conflicting objectives must be achieved during cerebral glioma surgery: (1) to obtain a tumor excision as complete as possible, the oncological prognosis being improved by surgery; and (2) to limit the risk of definitive neurological deficit by respecting the brain areas infiltrated by the tumor remaining functional. The objective of our work is to develop an intraoperative biomecanical analysis and a micro vascularization imaging method and validate the interest of these techniques for the diagnosis of tumor neo-angiogenesis and ultimately to target the surgical procedure during surgery.**

***Index Terms*—Brain, cerebral tumors, viscoelasticity, neo-angiogenosis, blood flow, sensitive Doppler, robust PCA, optimization.**

I. Introduction

Gliomas are tumors infiltrating healthy brain tissue and can be located near or in functional areas of the brain. Currently, the tumor is detected before surgery by morphological and vascular MRI. A neuronavigation system makes it possible to locate the position of this tumor in 3D thanks to a spatial positioning system linked to a stereotactic helmet. This allows the surgeon to precisely define the skull area to be opened at the front of the tumor. When the skull is opened, the "brain shift" phenomenon shifts the position of the tumor relative to preoperative MRI images and prohibits the use of neuronavigation for tumor resection. Thus, intraoperative ultrasound echography currently remains the real-time imaging method routinely used in the neurosurgery unit to delimit the area infiltrated by the tumor in the healthy brain. Our project aims to evaluate the interest of US elastography and intraoperative sensitive Doppler in the surgical management of brain tumors.

II. Materials and Methods

The French research ethics board approved our experimental protocol (CPPIDF1-2018-ND42-cat2. ELASTOGLI project). The brain tumor removal procedure takes place at the Regional University Hospital Bretonneaux of Tours, Department of Neurosurgery. Fig. 1 shows the operating room during the surgical operation. We can see the Brainlab NeuroNavigation system, the SuperSonic Imagine Aixplorer ultrasound scanner and the computer with the SonicLab V12 research pack to upload the sequences. The surgeon places the conventionnal SL10-2 ultrasound probe, composed by 192 elements on the area of the brain to be studied. Different strategies are used during the surgery. Firstly, we record the *in vivo* Bmode image, the Young modulus image and the AngioPlus power Doppler image with the commercial mode of the Aixplorer. Fig. 2 depicts the B-mode images (upper left) of a heterogeneous glioma. SWE imaging show a Young modulus of 11.2KPa in the center of the glioma and 41kPa in the left part of the glioma. Power Doppler imaging shows the glioma perfusion. We can clearly see the details of the tumor vasculature and a small area at the bottom of the image where the tumor is necrotic. This real-time commercial imaging mode allows us to select precisely the region of interest in the tumor for more advanced analysis using the research sequence.

Fig. 1. Operating room of the Neurosurgery department Tours hospital. We identify the Brainlab neuronavigation system, the US Aixplorer imaging system and the computer to upload the research sequences.

II.A. Shear Wave Spectroscopy (SWS)

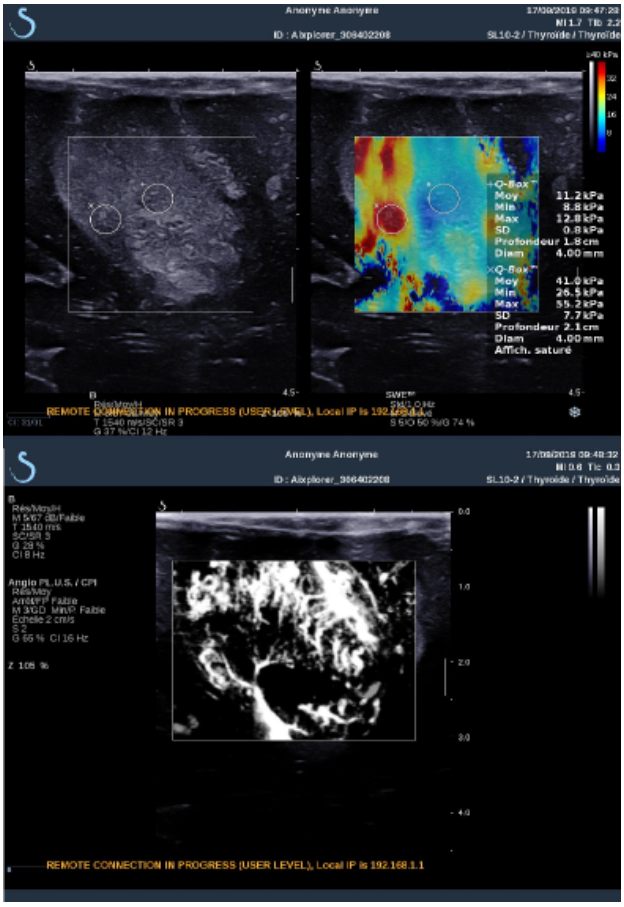

Fig. 2. B-mode, Young modulus and Power Doppler AngioPlus images of a heterogeneous cerebral glioma obtained *in vivo* with the Aixplorer commercial mode

We want to assess the frequency dependence of the shear wave speed inside a small region of the glioma. The SWE sequence is upload on the Aixplorer with the SonicLab software. The SWS experiment is based on two steps, the generation of the shear waves and ultrafast imaging of their propagation. For a detailed description of basic principles and phase estimation algorithm, the reader can refer to [1]. Data are transfered on a computer for off line beamforming and signal processing. Fig. 3 visualizes the Shear wave propagation induced inside the cerebral glioma by the US radiation force nonlinear effect. SW are presented at three different times (t1=0.29msec, t2=0.96msec and t3=1.7msec) superposed to the Bmode image at the same position than in Fig. 2. The Bmode image is obtained from the SWE sequence and has not the same quality than in Fig. 2. A small rectangle shows the region of interest. Axial lignes between 18.9mm and 19.8mm are summed and the SW is analysed from 20mm to 27mm in the lateral direction (corresponding to the rectangle in Fig. 3). SW elastogram is shown in Fig. 4. From a Voigt model, the elastic modulus $\mu = 2.2kPa (E = 6.6kPa)$ and the shear viscous modulus is $\eta = 0.7Pa.s$

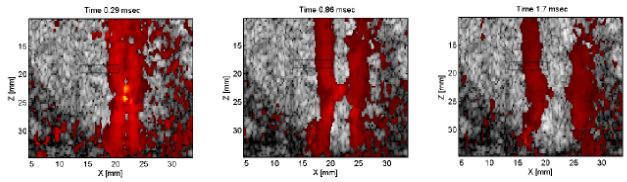

Fig. 3. Shear wave propagation induced inside the cerebral glioma by the US radiation force nonlinear effect. SW are presented at three different times (t1=0.29msec, t2=0.96msec and t3=1.7msec) superposed to the Bmode image at the same position than in Fig. 2

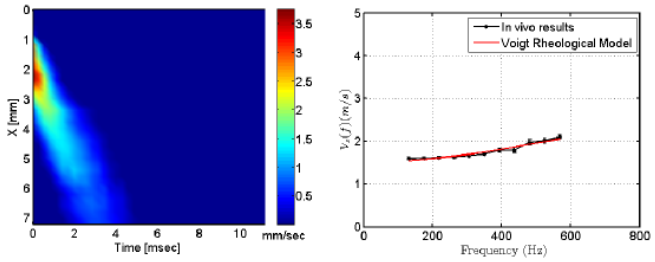

Fig. 4. Elastogram in Time t and space x domain and the SW dispersion in function of the frequency in the [131-568]Hz bandwidth. From a Voigt model we obtain $\mu = 2.2kPa (E = 6.6kPa)$ and the shear viscous modulus is $\eta = 0.7Pa.s$

II.B. Perfusion and tissue/noise filtering

A. RPCA Theory

Blood flow detection has been greatly improved by using ultrafast sequences associated with adaptive spatiotemporal singular values decomposition (SVD) clutter filtering [2]. Through this decomposition, the filtering strategy is based on empirical thresholding the correlation of spatial singular vectors magnitude. This leads to the separation of the subspaces corresponding to respectively the tissues and the blood flow [3]. The empirical choice of the optimal threshold is however not obvious in most of practical applications. An alternative solution consists in using robust principal component analysis (RPCA) techniques [4]–[7]. In order to improve these techniques, different attempts have been done in ultrasound imaging, either using sparse priors in a specific basis [8], or sparse coding through a specific dictionary [9]. In this paper we investigate a different way that adaptive SVD [3] for separating blood flow and tissues based on an inverse problem related to RPCA in order to obtain a high-sensitivity blood flow estimation.

We denote by $\boldsymbol{S} \in \mathbb{C}^{N_z N_x \times N_t}$ the Casorati matrix obtained from 3D IQ complex (number) Doppler data, recorded via ultrafast imaging, with depth N_z, probe width N_x and acquisition time N_t. The most common method used to filter the clutter and recover the blood flow consists in first performing singular value decomposition (SVD) of $\boldsymbol{S}$ and second setting two thresholds to identify the subspaces of blood, tissue (clutter) and noise, based on the corresponding singular values and vectors.

Alternatively, $\boldsymbol{S}$ can be modelled as:

$$\boldsymbol{S} = \boldsymbol{T} + \boldsymbol{B} + \boldsymbol{N}, \quad (1)$$

with $\boldsymbol{T} \in \mathbb{C}^{N_z N_x \times N_t}$ the tissue, $\boldsymbol{B} \in \mathbb{C}^{N_z N_x \times N_t}$ the blood, and $\boldsymbol{N} \in \mathbb{C}^{N_z N_x \times N_t}$ the noise matrices. Assuming that the blood (i.e., the flow) is sparse and the tissue weakly changes or moves over time, reasonable assumptions in most of practical applications, it is thus possible to estimate $\boldsymbol{B}$ from $\boldsymbol{S}$. Classically, sparsity is catched in a tractable manner by the l_1-norm and weak changes or high correlation by the nuclear norm $||.||_*$. This results in solving an inverse problem in which the estimation of $\boldsymbol{B}$ and $\boldsymbol{T}$, say $(\hat{\boldsymbol{B}}, \hat{\boldsymbol{T}})$, can be obtained by minimizing the following function:

$$(\hat{\boldsymbol{B}}, \hat{\boldsymbol{T}}) = \arg\min_{\boldsymbol{B},\boldsymbol{T}} ||\boldsymbol{S} - \boldsymbol{B} - \boldsymbol{T}||_F^2 + \lambda||\boldsymbol{B}||_1 + ||\boldsymbol{T}||_* \quad (2)$$

where $||.||_F^2$ is the Frobenus norm. $\lambda > 0$ is a hyper-parameter to be tuned, balancing the trade-off between the sparsity of the blood and low-rankness of the tissues. To solve the convex optimization problem above, many algorithms exist in the literature, such as the one proposed in [5]. This method is referred to as robust principal component analysis (RPCA). A comprehensive review and analysis of this kind of methods can be found in [10]. Some of these techniques have been revisited in ultrasound imaging by Bayat *et al.* [8] who solved this problem, assuming that $\boldsymbol{B}$ is sparse in the Fourier domain, or by Sathyanarayna *et al.* [9] who investigated the same problem via a sparse coding through expressing $\boldsymbol{B}$ in a specific dictionary.

One classical way for solving (2) is to use the Alternating Direction Method of Multipliers (ADMM) framework. ADMM aims at finding the solution of a complex optimization problem by accounting for easy-to-solve sub-problems. The minimization problem considered within ADMM is as follows:

$$(\hat{\boldsymbol{x}}, \hat{\boldsymbol{z}}) = \arg\min_{\hat{\boldsymbol{x}},\hat{\boldsymbol{z}}} f(\boldsymbol{x}) + g(\boldsymbol{z}) \quad s.t. \quad \boldsymbol{A}\boldsymbol{x} + \boldsymbol{B}\boldsymbol{z} = \boldsymbol{C} \quad (3)$$

where $f(\boldsymbol{x})$ and $g(\boldsymbol{z})$ are convex functions and $\boldsymbol{A}$, $\boldsymbol{B}$ and $\boldsymbol{C}$ are matrices of appropriate sizes. The augmented Lagrangian associated to (3) is:

$$\begin{aligned} L(\boldsymbol{x}, \boldsymbol{z}, \boldsymbol{\nu}) &= f(\boldsymbol{x}) + g(\boldsymbol{z}) + \boldsymbol{\nu}^T(C - A\boldsymbol{x} - B\boldsymbol{z}) + \frac{\mu}{2}||C - A\boldsymbol{x} - B\boldsymbol{z}||_2^2 \\ &\approx f(\boldsymbol{x}) + g(\boldsymbol{z}) + \frac{\mu}{2}||C - A\boldsymbol{x} - B\boldsymbol{z} + \frac{1}{\mu}\boldsymbol{\nu}||_2^2 \end{aligned} \quad (4)$$

The main idea of ADMM is to minimize the augmented Lagrangian above by iteratively processing the following three steps (k stands for the iteration number) until convergence:

Step 1: $\hat{\boldsymbol{x}}^{(k+1)} = \arg\min_{\hat{\boldsymbol{x}}} L(\boldsymbol{x}, \boldsymbol{z}^{(k)}, \boldsymbol{\nu}^{(k)})$;
Step 2: $\hat{\boldsymbol{z}}^{(k+1)} = \arg\min_{\hat{\boldsymbol{z}}} L(\boldsymbol{x}^{(k+1)}, \boldsymbol{z}, \boldsymbol{\nu}^{k})$;
Step 3: $\boldsymbol{\nu}^{(k+1)} = \boldsymbol{\nu}^{(k)} + \mu(C - A\boldsymbol{x}^{(k+1)} - B\boldsymbol{z}^{(k+1)})$.

Applying ADMM to (2) leads to the following augmented Lagrangian:

$$L(\boldsymbol{B}, \boldsymbol{T}, \boldsymbol{\nu}) = \lambda||\boldsymbol{B}||_1 + \rho||\boldsymbol{T}||_* + \frac{\mu}{2}||\boldsymbol{S} - \boldsymbol{B} - \boldsymbol{T} + \frac{1}{\mu}\boldsymbol{\nu}||_2^2 \quad (5)$$

Finally, at each iteration, RPCA algorithm consists in the following three steps:

- Step 1: $\hat{\boldsymbol{B}}^{(k+1)} = \arg\min_{\hat{\boldsymbol{B}}}(\lambda||\boldsymbol{B}||_1 + \frac{\mu}{2}||\boldsymbol{B} - (\boldsymbol{S} - \boldsymbol{T}^{(k)} + \frac{1}{\mu}\boldsymbol{\nu}^{(k)})||_2^2)$;
- Step 2: $\hat{\boldsymbol{T}}^{(k+1)} = \arg\min_{\hat{\boldsymbol{T}}}(||\boldsymbol{T}||_* + \frac{\mu}{2}||\boldsymbol{T} - (\boldsymbol{S} - \boldsymbol{B}^{(k+1)} + \frac{1}{\mu}\boldsymbol{\nu}^{(k)})||_2^2)$;
- Step 3: $\boldsymbol{\nu}^{(k+1)} = \boldsymbol{\nu} + \mu(\boldsymbol{S} - \boldsymbol{B}^{(k+1)} - \boldsymbol{T}^{(k+1)})$.

Note that steps 1 and 2 above are both convex problems having closed-form solutions: soft thresholding [11] for step 1, and singular value thresholding (SVT) [12] for step 2. We can mention that our algorithm does not explicitly take into account the limited resolution of Doppler data caused by the system impulse response (i.e., the PSF). Very recent work of [13] proposed a joint deconvolution and RPCA inverse problem for filtering but this method is not addressed in this work.

B. Experimental glioma perfusion

A sequence consisting of 3 tilted plane waves [-5, 0, +5] obtained at a frame rate of 3 kHz during 1 s was uploaded in the Aixplorer. After compounding, the resulting image frame rate is PRF=1kHz. Acquired data were exported for off-line processing. Note that the thresholds used within SVD were manually tuned to their best values. Fig. 6 shows the Power Doppler summed from the 1000 filtered complex IQ frames. Our perfusion results are not unfortunately obtained during the same acquisition than the SWE part of this paper. These data on Fig. 6 have been obtained from a previous brain surgery. The tumor is situated from the distance 5mm to 30mm depth. Some fine vascularisation is visible on the upper part of the tumor which is not very vascularized. A central region is necrotic between 17mm and 23mm with a circular shape. On the lower part of the tummor, we can see that this Power Doppler image shows a fine vascularization. The image has the same dynamic (-50dB) for comparison and with a fixed value μ and η in (5). RPCA image seems little more noisier than the SVD method on the lower region of the image.

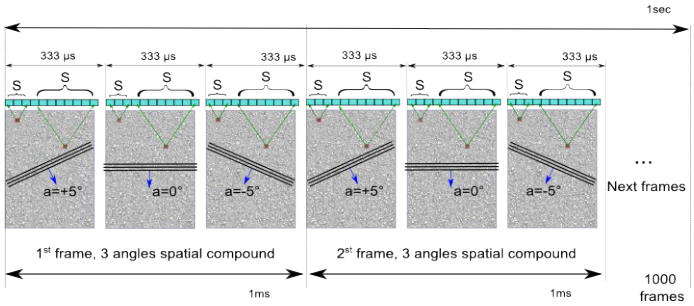

Fig. 5. Sensitive Doppler sequence consisting in 3 tilted US plane waves [-5, 0, +5] obtained at a frame rate of 3 kHz during 1 s. After compounding, the resulting image frame rate is PRF=1kHz.

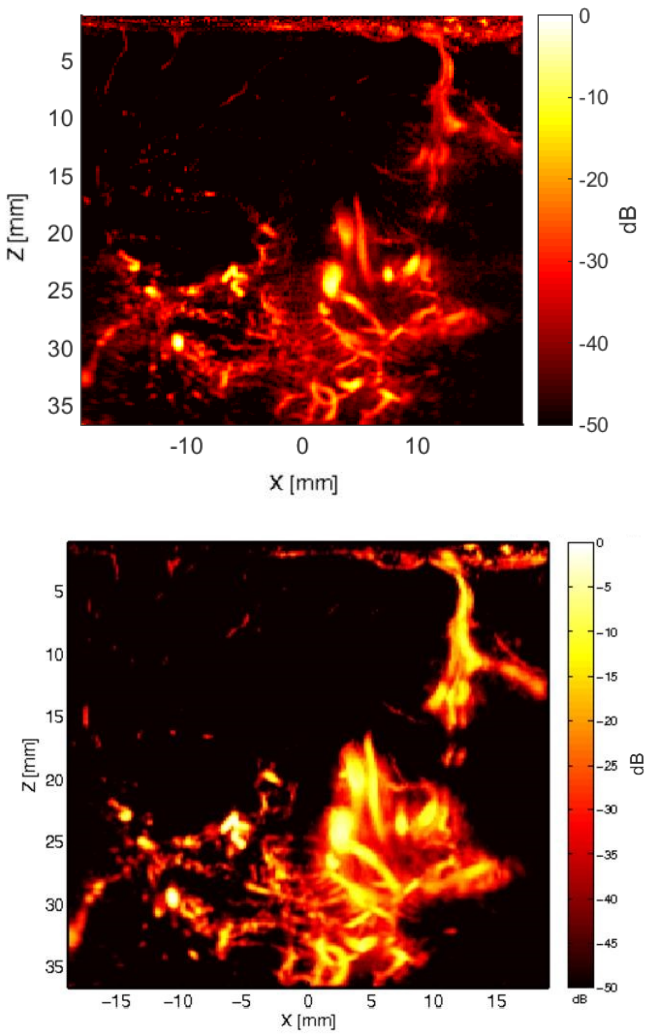

Fig. 6. *In vivo* Perfusion image of a cerebral glioma:(upper) Power Doppler with SVD method, (lower) Power Doppler with RPCA method

III. Conclusion

We present the research that we are conducting on tumors *in vivo* during surgery. We propose to characterize the viscoelastic behavior of the a small tumor ROI through a Voigt model applied on the SW speed dispersion curve in function of the frequency. The tumor is heterogeneous in terms of Bmode and elasticity image. We will correlate these data with the grade of the tumor obtained by histology. The SWE sequence associated with our phase estimation algorithm is well applied to this problem. The dispersion curve is of good quality in our analysis bandwidth. For perfusion, the sensitive sequence with 1000 temporal resulting beamformed IQ data give enough sensibility to visualize the small vessels inside the tumors. Two methods for blood and tissue-sub-space separation were compared in this work. SVD is a straightforward and easy-to-implement method, based on the correlation of spatial singular vectors magnitude. However, it requires a manual tuning of the two thresholds needed to separate tissue, blood and noise components, to visualize only the blood flow. From this perspective, SVD may not be reproducible from one operator to another. The selection of blood directly depends on the selection of these thresholds, without any further control on the result. RPCA algorithm is more complex than classical SVD, It estimates the two main components, tissue and blood, by exploiting their low-rank or sparse properties, leading to an automatic method without the need of manually tuning the parameters. And for the same sequences, we find that RPCA yields the same result if there is no change in the parameters λ and μ. Moreover, it has parameters on which one can play to optimize the result. This method is therefore more advantageous and easier to handle and we are still in the process of improving this method. We are currently conducting *in vitro* flow phantom tests to accurately quantify the quality of the different filtering methods we are developing.

in vitro

References

[1] T. Deffieux, G. Montaldo, and Fink. Tanter, M, "Shear wave spectroscopy for in vivo quantification of human soft tissues visco-elasticity," *IEEE Transactions on Medical Imaging*, vol. 28, no. 3, pp. 313–, Mar. 2009.

[2] C. Demené, T. Deffieux, M. Pernot, B. F. Osmanski, V. Biran, J. L. Gennisson, L. A. Sieu, A. Bergel, S. Franqui, J. M. Correas, I. Cohen, O. Baud, and M. Tanter, "Spatiotemporal clutter filtering of ultrafast ultrasound data highly increases doppler and fultrasound sensitivity," *IEEE Transactions on Medical Imaging*, vol. 34, no. 11, pp. 2271–2285, Nov. 2015.

[3] J. Baranger, B. Arnal, F. Perren, O. Baud, M. Tanter, and C. Demené, "Adaptative spatiotemporal svd clutter filtering for ultrafast doppler imaging using similarity of spatial singular vectors," *IEEE Transactions on Medical Imaging*, vol. 37, no. 7, pp. 1574–1586, July 2018.

[4] R. A. Maronna, "Robust m-estimators of multivariate location and scatter," *Ann. Stat.*, vol. 4, no. 1, pp. 51–67, 1976.

[5] J. Wright, A. Ganesh, S. Rao, Y. Peng, and Y. Ma, "Robust principal component analysis: Exact recovery of corrupted low-rank matrices via convex optimization," *Proc. Neural Inf. Process. Syst*, pp. 1–9, 2009.

[6] F. Torre and M. Black, "Robust principal component analysis for computer vision," *Proc. Int. Conf. Comput. Vis.*, pp. 362–369, 2001.

[7] S. J. Devlin, R. Gnanadesikan, and J. R. Kettenring, "Robust estimation of dispersion matrices and principal components," *J. Amer. Stat. Assoc.*, vol. 76, no. 374, pp. 354–362, 1981.

[8] M. Bayat and M. Fatemi, "Concurrent clutter and noise suppression via low rank plus sparse optimization for non-contrast ultrasound flow doppler processing in microvasculature," in *IEEE International Conference on Acoustics, Speech and Signal Processing ICASSP'2018*, Calgary, Canada, 2018.

[9] S. G. Sathyanarayna, S. T. Acton, and J. A. Hossack, "Suppression of clutter by rank adaptive reweighted sparse coding," in *IEEE International Ultrasonics Symposium IUS'2017*, Washington DC, USA, 2017.

[10] Thierry Bouwmans, Andrews Sobral, Sajid Javed, Soon Ki Jung, and El-hadi Zahzah, "Decomposition into low-rank plus additive matrices for background/foreground separation: A review for a comparative evaluation with a large-scale dataset," *Computer Science Review*, vol. 23.

[11] Z. Lin, M. Chen, L. Wu, and Y. Ma, "The augmented lagrange multiplier method for exact recovery of corrupted low-rank matrices," *Dept. Electr. Comput. Eng., UIUC, Urbana, Tech. Rep.*, 2009.

[12] J. Cai, E. J. Candès, and Z. Shen, "A singular value thresholding algorithm for matrix completion," *Soc. Ind. Appl. Math. J. Optim.*, vol. 20, no. 4, pp. 1956—1982, 2010.

[13] H. Shen, C.Barthelemy, E.Khoury, I.Zemmoura, JP.Remeniéras, A.Basarab, and D.Kouamé, "High-resolution and high-sensitivity blood flow estimation using optimization approaches with application to vascularization imaging," in *IEEE International Ultrasonics Symposium IUS'2019*, Glasgow, UK, Oct. 2019.